Nanoscale

RSC Publishing

PAPER

View Article Online
View Journal | View Issue

Cite this: *Nanoscale*, 2013, **5**, 3022

SnO_2@CdS nanowire-quantum dots heterostructures: tailoring optical properties of SnO_2 for enhanced photodetection and photocatalysis

Jun Pan,*[a] Jiangtian Li,[b] Zilai Yan,[a] Banghong Zhou,[a] Hanshuo Wu[a] and Xiang Xiong*[a]

Received 14th December 2012
Accepted 3rd February 2013

DOI: 10.1039/c3nr34096a

www.rsc.org/nanoscale

Rationally designed SnO_2@CdS nanowire-quantum dots (QDs) heterostructures were realized by a wet-chemical method *via* hydroxide cluster growth mechanism on high crystalline quality SnO_2 nanowires, which were synthesized by a vapor transport method. The heterostructures showed enhanced photon harvesting capability and photodetection sensitivity at visible regime than that of wide band gap homogeneous SnO_2 nanowires, as characterized by UV-Vis absorption and photoconductivity measurements. In addition, the SnO_2@CdS nanowire-QDs heterostructures showed enhanced photocatalytic activity by more than 109% in a conceptual demonstration of photodegradation of methylene blue solution. Our results suggest that the SnO_2@CdS nanowire-QDs heterostructures exhibit considerable promise for highly sensitive visible-light photodetectors and highly efficient photocatalysis.

Introduction

One-dimensional (1D) metal oxide nanowires, particularly wide band gap transparent conducting oxide nanowires such as those from zinc, titanium, indium and tin oxides, exhibit considerable promises in photonics, photocatalysis and photovoltaics.[1–4] With large scale arrays readily achievable, the electrical and optical properties of the nanowires can be tailored towards highly efficient light harvesting.[5–7] However, the wide band gap nature of those materials is suitable only for light harvesting in the UV regime, leaving poor efficiency in the visible region.[8] A solution to this problem is to combine metal oxide semiconductors with sensitizers of narrow band gap materials to extend their absorption range.[9,10] As a potential sensitizing strategy, semiconductor QDs show unique advantages of strong size-dependence of band gap, thus enabling full tunability even with a single QD material.[11,12] Higher efficiency can also be achieved by utilizing electrons to generate multiple electron–hole pairs with a single high-energy photon through the impact ionization effect.[13]

SnO_2 is one of the most promising materials with its well-known excellent transparency, conductivity, and geological abundance. It has been widely used in many fields such as electronics,[14] gas sensors,[15] energy storage,[16] and energy conversion.[17] However, the relatively wide band gap nature (E_g = 3.7 eV at 300 K) limits its applications in nanophotonics and photocatalysis.

In this work, we explore an effective quantum dot sensitization scheme based on CdS QDs decoration of high quality SnO_2 nanowires synthesized by chemical vapor deposition (CVD). CdS QDs with a narrower band gap (E_g = 2.4 eV, at 300 K) was chosen as light harvesters in visible regime. We propose the photoresponse mechanism of the SnO_2@CdS nanowire heterostructures as shown in Fig. 1. The band alignment was drawn according to the photoelectron spectroscopy study by Fritsche *et al.*[18] A slight depletion region is formed upon equilibrium to prevent further carrier exchange. An electron–hole pair is generated after the absorption of a photon with energy larger than the band gap of CdS QDs. Subsequently, the photogenerated electrons diffuse to the conduction band of coupled SnO_2 nanowires because of concentration gradient. The photogenerated hole in the CdS QDs can migrate to the surface and

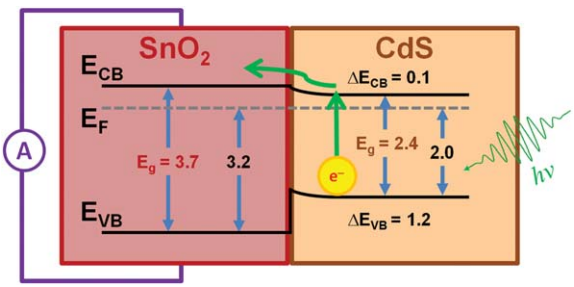

Fig. 1 Schematic of the photoresponse mechanism of SnO_2@CdS nanowire-QDs heterostructure.

[a]*State Key Laboratory for Powder Metallurgy, Central South University, Changsha 410083, China. E-mail: xiongx@csu.edu.cn; jun.pan@csu.edu.cn*

[b]*Department of Mechanical and Aerospace Engineering, West Virginia University, Morgantown, WV, 26506-6106, USA*

participate in the oxidation of adsorbed organics. The electrons that are transferred to the conduction band of SnO_2 contributed dominantly to the enhancement of photoconductive characteristics below the SnO_2 nanowire band gap. Meanwhile, the SnO_2@CdS nanowire heterostructures were also used as the photoanodes materials for the solar cells owing to higher recombination resistances, faster charge transport, and more efficient charge separation.[19,20]

To realize the rationally designed SnO_2@CdS nanowire heterostructures, CdS QDs were synthesized *via* a chemical bath deposition method (CBD) on single crystalline SnO_2 nanowires grown by a vapor transport method. Photoconductive characteristics and photocatalytic properties of SnO_2@CdS nanowire heterostructures were then investigated systematically.

Experimental section

Synthesis and characterization of nanostructures

SnO_2 nanowires were synthesized by a vapor transport method with a feedstock source of SnO_2 powder (purity 99.99%). The source powder was loaded into an alumina boat and placed 10 cm upstream from the Au-coated Al_2O_3 substrate in a quartz tube, which was centered in a horizontal tube furnace. The tube was evacuated by a rotary pump to a base pressure of 10^{-2} Torr. Prior to the heating, high-purity Ar was used to flush the quartz tube. Then, the furnace was heated to 825 °C and maintained for 30 min under a constant Ar gas flow (40 sccm) at a total pressure of 50 Torr.

CdS quantum dots (QDs) were deposited on the surface of SnO_2 nanowires *via* a chemical bath deposition. 2 mM CdS precursor solution was prepared by dissolving $CdSO_4$ and thiourea (with a molar ratio of Cd^{2+} to $S^{2-} = 5:1$) in ammonia solution. Morphology and QDs coverage can be controlled by the concentration of ammonia solution. By varying the different concentrations of ammonia solution (1 M and 2 M), sparsely covered and heavily covered heterostructures can be obtained respectively. SnO_2 nanowires were cleaned with N_2 flow and then immersed into CdS precursor solution. The solution was put into an oil bath at 60 °C for 30 min. Then, SnO_2 nanowires were immediately taken out and washed with deionized water and ethanol. Finally, the heterostructures were annealed at 400 °C under vacuum for 2 h to enhance the interaction between CdS and SnO_2.

The heterostructures were thus collected and characterized by field-emission scanning electron microscopy (FESEM, JEOL JSM-7001F), X-ray powder diffraction (XRD, Bruker D8 advanced diffractometer, CuK_α radiation), transmission electron microscopy (TEM, JEOL JEM-2100), UV/Vis/NIR Spectrometer (PerkinElmer Lambda 950) and Micro Raman Spectroscopy (Horiba JY T64000).

Preparation of single nanostructure photodetectors

To fabricate the single nanostructure device, SnO_2 nanowires and SnO_2@CdS nanowire heterostructures were dispersed on a Si substrate with an oxide layer of 300 nm. The source–drain contacts were patterned by electron beam lithography on a layer of poly(methyl methacrylate) resist. Ti (60 nm) and Au (40 nm) layers were deposited sequentially by thermal evaporation followed by a lift-off process in acetone. The nanowires were etched in diluted HF solution (5%) 10 seconds to remove amorphous oxide layer and CdS surface layer to expose crystalline SnO_2 core. A rapid thermal annealing at 250 °C was carried out in forming gas for 1–3 min to obtain Ohmic contact. The top inset in Fig. 5b shows the typical device image with a channel width of 1 μm.

Measurements of photoconductive characteristics

The *I–V* curves of SnO_2 nanowire and SnO_2@CdS nanowire heterostructure in dark were measured under the DC mode. Photoconductivity measurements were carried out on a home-made setup as schematically shown in Fig. 5a. A halogen lamp and a monochromator were combined to provide monochromatic light. The monochromatic light was split into two beams: one beam was used to monitor the intensity of light detected by a pyroelectric detector, and the other beam was shined on the sample. The photocurrent signal was amplified by a current preamplifier and then collected by a lock-in amplifier (SR830) with a chopper providing reference signal. Hence, in photocurrent measurement the dc current was filtered by the lock-in amplifier and only photo-generated current was measured.

Measurements of photocatalytic properties

The photocatalytic activities of the samples were tested by the decomposition of methylene blue in an ATLAS Suntest CPS+. The as-prepared samples (pure SnO_2 nanowires and CdS quantum dot decorated SnO_2 nanowires on Al_2O_3 substrate) were separately immersed into two cuvettes filled with 25 ml aqueous suspension of methylene blue. The cuvettes were exposed to light in the spectral range from 310 to 800 nm with an intensity of 100 mW cm^{-2}. The sample compartment was water-cooled to maintain the thermal stability of methylene blue. The UV-Vis spectroscopy (PerkinElmer Lambda 950) was then measured as a function of illumination time, in which the absorbance evolution reflects the change of methylene concentration.

Results and discussion

CBD of CdS QDs has been widely studied for the various compositions of chemical solutions.[21] QDs can be grown directly on the surface of nanowires with the CBD method by the solution of cadmium salt ($CdSO_4$), aqueous ammonia (complexing agent), and thiourea (NH_2CSNH_2, sulfur source) in this work. The general reaction pathways for the CdS formation in thiourea chemical bath are illustrated in the following steps:

$$NH_3 + H_2O \leftrightarrow NH_4^+ + OH^- \quad (1)$$

$$Cd^{2+} + 4NH_3 \leftrightarrow Cd(NH_3)_4^{2+} \quad (2)$$

$$(NH_2)_2CS + OH^- \rightarrow CH_2N_2 + H_2O + HS^- \quad (3)$$

$$HS^- + OH^- \rightarrow S^{2-} + H_2O \quad (4)$$

$$Cd^{2+} + S^{2-} \rightarrow CdS \quad (5)$$

$$Cd^{2+} + 2OH^- \rightarrow Cd(OH)_2 \quad (6)$$

$$Cd(OH)_2 + S^{2-} \rightarrow CdS + 2OH^- \quad (7)$$

In the process, ammonia produces a hydroxide ion and forms a cadmium tetramine complex by two different equilibrium reactions ((1) and (2)). Ammonia can maintain a slightly basic pH of the solution, thus preventing violent cadmium hydroxide formation. In an alkaline solution, thiourea decomposes and generates free sulfur ions ((3) and (4)). CdS might form through an ion-by-ion mechanism (5) or a hydroxide cluster mechanism ((6) and (7)), either exclusively or concurrently, on the surface of SnO_2 nanowires.

By varying the different concentrations of ammonia solution (1 M and 2 M), two different heterostructure morphologies which correspond to different level of QDs coverage on the nanowires can be observed. Fig. 2 shows the typical SEM and TEM images of the sparsely covered nanowires from CBD with higher ammonia concentration (a–c) and the heavily covered nanowires from CBD with lower ammonia concentration (d–f). The presence of such coverage evolution implies that the hydroxide cluster mechanism was the dominant pathway under our experimental conditions as the direct ion-by-ion mechanism should not strongly depend to ammonia concentration, which on the other hand correlates negatively with the formation of cadmium hydroxide essential for the hydroxide cluster mechanism. Meanwhile, such result also demonstrate the possibility for well-controlled QDs coverage on SnO_2 nanowires *via* the CBD method.

High-resolution TEM analysis of SnO_2@CdS nanowire heterostructures reveals that SnO_2 nanowire and CdS QDs are crystalline. CdS QDs clusters with a diameter of ~10 to 20 nm are identified which are homogeneously dispersed on the surface of SnO_2 nanowires with a diameter of ~35 nm. Clear lattice fringes are observed as shown in Fig. 2c and f. The measured spacing of the crystallographic planes is 2.69 nm, corresponding to the rutile-structured SnO_2 crystal, suggesting that CVD-grown SnO_2 nanowires had a preferred growth orientation along ⟨101⟩. Moreover, clear lattice fringes of CdS QDs are resolved to be 3.16 nm and 3.36 nm, corresponding to the (101) and (002) planes of hexagonal crystal structure CdS, respectively.

The crystalline structures of the SnO_2@CdS nanowire heterostructures are further identified *via* XRD as shown in Fig. 3. Although the diffraction peaks of CdS are much weaker compared to the high-intensity peaks of as-grown well-crystallized SnO_2 nanowires, those XRD peaks can be indexed as the hexagonal crystalline structure CdS (Fig. 3a) in agreement with the TEM observation.

Raman scattering spectroscopy is another powerful and yet non-destructive method to probe crystalline quality,[22] phase impurities,[23] structural modulation[24] or confined phonon states in nanowires.[25] Therefore, Raman scattering is used further to study the crystalline structures of SnO_2@CdS nanowire heterostructures. Fig. 3b shows the room-temperature Raman

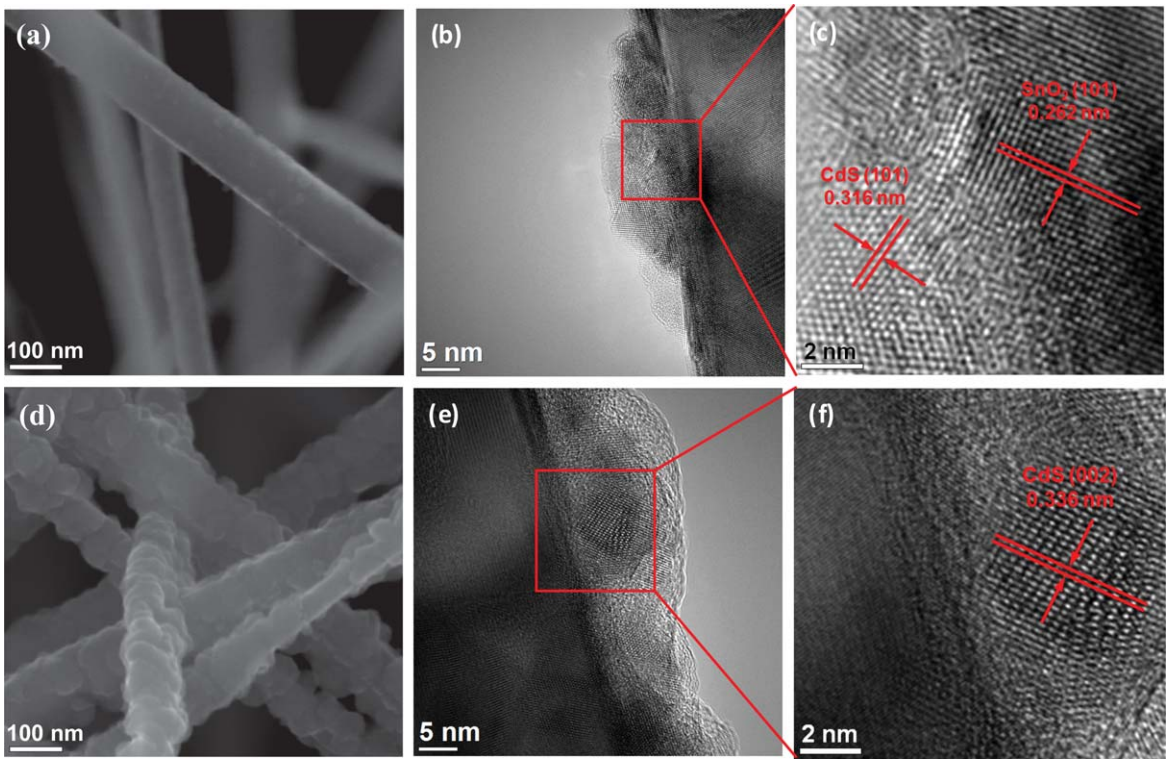

Fig. 2 SEM (a and d) and TEM images of (b, c, e and f) sparsely covered (upper row) and heavily covered (lower row) SnO_2@CdS nanowire heterostructures.

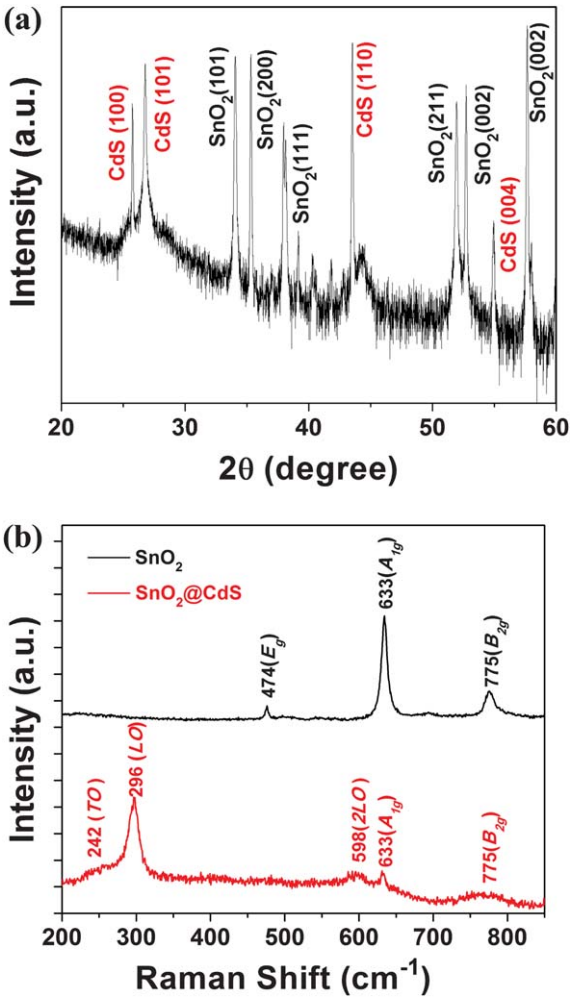

Fig. 3 (a) XRD spectrum of SnO_2@CdS nanowire heterostructures. The intensity is shown in log scale in order to bring CdS peaks more prominent. (b) Raman spectra of SnO_2 nanowires and SnO_2@CdS nanowire heterostructures.

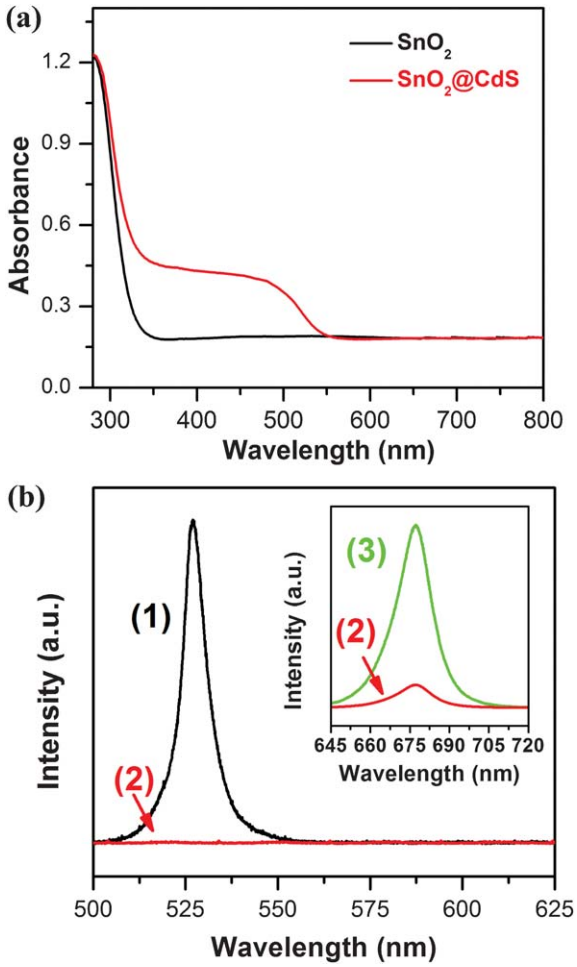

Fig. 4 (a) UV-Vis optical absorption spectra and (b) PL spectra of SnO_2 nanowires (plot 1) and SnO_2@CdS nanowire heterostructures (plot 2). PL spectrum of CdS QDs (plot 3) was used for comparison.

scattering spectra of SnO_2 nanowires and SnO_2@CdS nanowire heterostructures excited by a 457 nm laser line of an Argon ion laser. Three fundamental Raman scattering peaks of SnO_2 nanowires at 474, 633 and 775 cm^{-1} are identified, corresponding to the E_g, A_{1g} and B_{2g} vibrational modes, respectively.[26] Thus, these peaks further confirm that the SnO_2 nanowires possess tetragonal rutile structure. Three peaks of SnO_2@CdS nanowire heterostructures are clearly observed at 242, 296 and 598 cm^{-1}, corresponding to the TO mode, LO mode and 2LO mode of CdS.[27] It is noteworthy that the peak intensities at 633 and 775 cm^{-1} from SnO_2 nanowires have been significantly reduced, presumably because the covering of CdS nanocrystals extinct both excitation laser intensity and emitted Raman signals significantly.

Fig. 4a shows the UV-Vis optical absorption spectra taken at room temperature. SnO_2 nanowires show an absorption edge around 350 nm, which corresponds to the SnO_2 band edge absorption. The sharp absorption edge indicates that SnO_2 nanowires grown by CVD exhibit high crystalline quality. On the contrary, SnO_2@CdS nanowire heterostructures shows two absorption edges around 350 and 520 nm, corresponding to the band edges of SnO_2 and CdS respectively. The SnO_2@CdS nanowire heterostructures shows considerable increase of absorption in the spectrum regime of 320–520 nm, compared to pure SnO_2 nanowires. This enhancement of the light harvesting is due to the CdS quantum dots decoration.

Fig. 4b showed photoluminescence (PL) spectra of SnO_2 nanowires (plot 1) and SnO_2@CdS nanowire heterostructures (plot 2). For the pristine SnO_2 nanowires, a strong band edge emission can be clearly found at 527 nm with negligible emission peaks associated with deep-level defects, despite the large surface area of the SnO_2 nanowires. After CdS QDs deposition, significant quenching of the SnO_2 band edge emission was observed, implying that charge separation took place before the electron–hole recombination process may occur within CdS.[28] In addition, the band edge emission of CdS (inset, plot 2) is also largely depressed compared to the CdS QDs (inset, plot 3). The drastic quenching of the band edge emission for both SnO_2 and CdS in the heterostructure configuration is reasonable, considering the band alignment between SnO_2 and probability within both SnO_2 and CdS.[29] An advantage of our synthetic method is that the CdS QDs grow directly on the SnO_2 surface,

which improves the charge injection from CdS to SnO_2 and promotes the separation of hole–electron pairs at the interface.[30]

Photoconductivity measurement is performed on individual nanowire to investigate whether the enhanced absorption due to CdS QD decoration indeed results into more carrier injection. The experimental setup is schematically shown in Fig. 5a. Fig. 5b shows photocurrent measurements of a field effect transistor device from an individual SnO_2 nanowire and a SnO_2@CdS nanowire heterostructure with/without 355 nm light illumination, the DC current was filtered by the lock-in amplifier. The linear curves of both photocurrent and DC dark current (bottom inset in Fig. 5b) suggest good ohmic contacts of the devices. It is important to note that the increase of photocurrent of SnO_2 FET due to light illumination is negligible; however the photocurrent increases significantly in SnO_2@CdS nanowire heterostructure FETs. In addition, the increase of photoconductance, *i.e.*, the slope in the linear photocurrent curves, of SnO_2@CdS nanowire heterostructure FET is approximately 6 times larger than that of pristine SnO_2 nanowire under the same illumination. Hence, the enhancement of the photocurrent is due to the additional carrier injection from CdS QDs to the SnO_2 nanowire backbone. Photogenerated electrons from CdS diffuse into SnO_2, forming an accumulation layer of electrons in the potential well adjacent to the interface of the SnO_2@CdS heterojunction, resulting in the enhanced photocurrent.[31]

The plot of photocurrent (I) measured at various light intensity (P) is given in Fig. 5c. A power law dependence can fit the relation of I *vs.* P quite well for all intensities:[32,33]

$$I = AP^r \tag{8}$$

where A is a constant for a certain wavelength, and exponent r determines the response of photocurrent to light intensity. Fitting eqn (8) to the curves yields $r = 0.888$ and 0.594, respectively, for the SnO_2@CdS nanowire heterostructure and SnO_2 nanowire. The non-unity exponent is observed for ZnO nanowires and CdS nanoribbons,[31,34] which is a result of the complex process of electron–hole generation, trapping, and recombination within the semiconductor.[32,35]

Fig. 5d shows the spectral response of a single SnO_2 nanowire and a SnO_2@CdS nanowire heterostructure as a function of wavelength. The inset is a semi-logarithmetic plot of the same spectra. In order to exclude the influence from the change of light intensity incident at the different wavelength, the responsivity of spectral response is normally used rather than photocurrent.[36] The responsivity (R) can be expressed as:

$$R = \frac{I}{P} \tag{9}$$

where I is the photocurrent and P is the light power shining on the device. However, responsivity may vary greatly from device

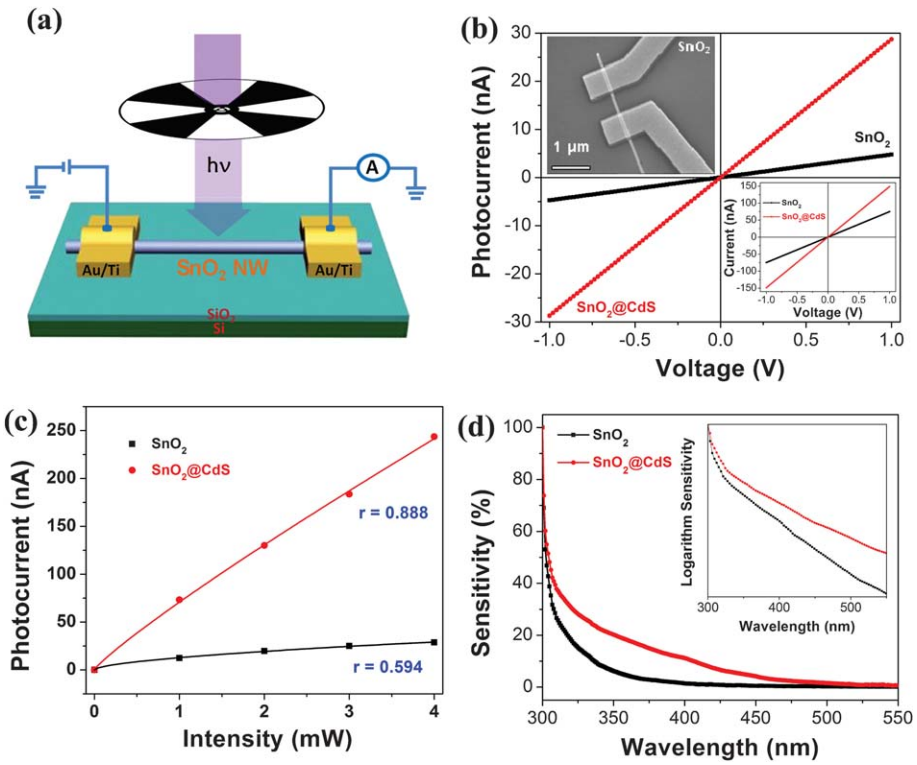

Fig. 5 (a) Schematic diagram of the photocurrent measurement. Photogenerated current was measured by a lock-in amplifier combined with an optical chopper. (b) Photocurrent of single SnO_2 nanowire and SnO_2@CdS nanowire heterostructure devices, illuminated by a 355 nm laser with an intensity of 0.5 mW cm^{-2}. The top inset to (b) shows an SEM image of a typical single nanowire device, the bottom inset shows the DC I–V curves of SnO_2 nanowire and SnO_2@CdS nanowire heterostructure in dark. (c) Variation of photocurrent of single SnO_2 nanowire and SnO_2@CdS nanowire heterostructure at different light intensities. The curves are fitted well by a power law. (d) Spectral response of single SnO_2 nanowire and SnO_2@CdS nanowire heterostructure. The inset is the same data plotted as a logarithm sensitivity.

to device so that it is inconvenient to create a meaningful comparison. One alternative is to take the normalization of the responsivity, which is called "*sensitivity*".[37] It is clearly revealed that, photoresponse can be obtained for the SnO_2 nanowire device when illuminating light with a wavelength larger than 350 nm negligible. Meanwhile the photocurrent has been detected even when the wavelength of the incident light is as long as 500 nm for SnO_2@CdS nanowire heterostructure.[38,39] This is direct evidence that CdS nanocrystal indeed contributed to the photocurrent. For the wavelength of the incident light less than the band gap of SnO_2 (around 350 nm), the electron–hole pairs cannot be excited and no photocurrent should be observed.[40] The origin photocurrent of SnO_2@CdS nanowire heterostructure in the wavelength ranging from 500 nm to 350 nm is due to the electrons transferred from CdS nanocrystal, which can be excited by the incident light. This result is also consistent with the absorption spectra shown in Fig. 4. Besides, the sensitivity of SnO_2@CdS nanowire heterostructure is still larger than that of mere SnO_2 nanowire. The enhanced sensitivity might be attributed to the CdS nanocrystal enhanced absorption, owing to the nanocrystal provides another absorption channel, which was verified from the absorption spectra. Since the measurements were performed at a constant light intensity, that is, constant product of photon energy and photon density per unit time, the photon density decreases with the wavelength decreases. Consequently the photon-induced carrier concentration also decreases (assuming one photon generates an electron–hole pair).[41] This conclusion is also in good agreement with photocurrent measurements (Fig. 5b).

The photocatalytic activities of the SnO_2 nanowire and the SnO_2@CdS nanowire heterostructure are tested by decomposition of a methylene blue solution. Fig. 6a and b shows the time evolution of the UV-Vis spectra of methylene blue when it is in contact with as-prepared SnO_2 and SnO_2@CdS nanostructures, respectively. To quantify the photoactivity of the nanomaterials, the absorbance *vs.* time (Fig. 6c) is plotted and fitted with an exponential decay:

$$N(t) = N_0 e^{-ct} \tag{10}$$

where c is the decay rate and N_0 is the initial concentration which correspond to the absorbance. The decay rates of SnO_2 and SnO_2@CdS samples are 0.021 and 0.044 min^{-1} respectively. The photocatalytic activity of the SnO_2@CdS nanowire heterostructures increases by more than 109% with respect to the SnO_2 nanowires. The photocatalytic decolorization of methylene blue is an apparent first-order reaction as verified by the linear transforms $\ln [C_0/C] = f(t)$ illustrated in the inset in Fig. 6c. The promising photocatalytic performance for the CdS QDs sensitized SnO_2 nanowires can be attributed to its narrow band gap CdS decoration. The narrow band gap CdS QD decoration enables the harvesting of solar spectrum in visible regime, making the SnO_2@CdS heterostructure a promising photocatalyst for solar-driven applications.[42] Meanwhile, the decorated CdS QDs will not only supply more active sites for the degradation reaction of organic compounds, but also enhance light harvesting through multiple scattering[43] and effectively promote the separation efficiency of the electron–hole pairs.[44] Additionally, chemical reactions are most effective when the transport paths through which molecules move into or out of the nanostructured materials are included as an integral part of the architectural design, as accomplished in our study by the QDs-decorated nanowire heterostructure.[45,46]

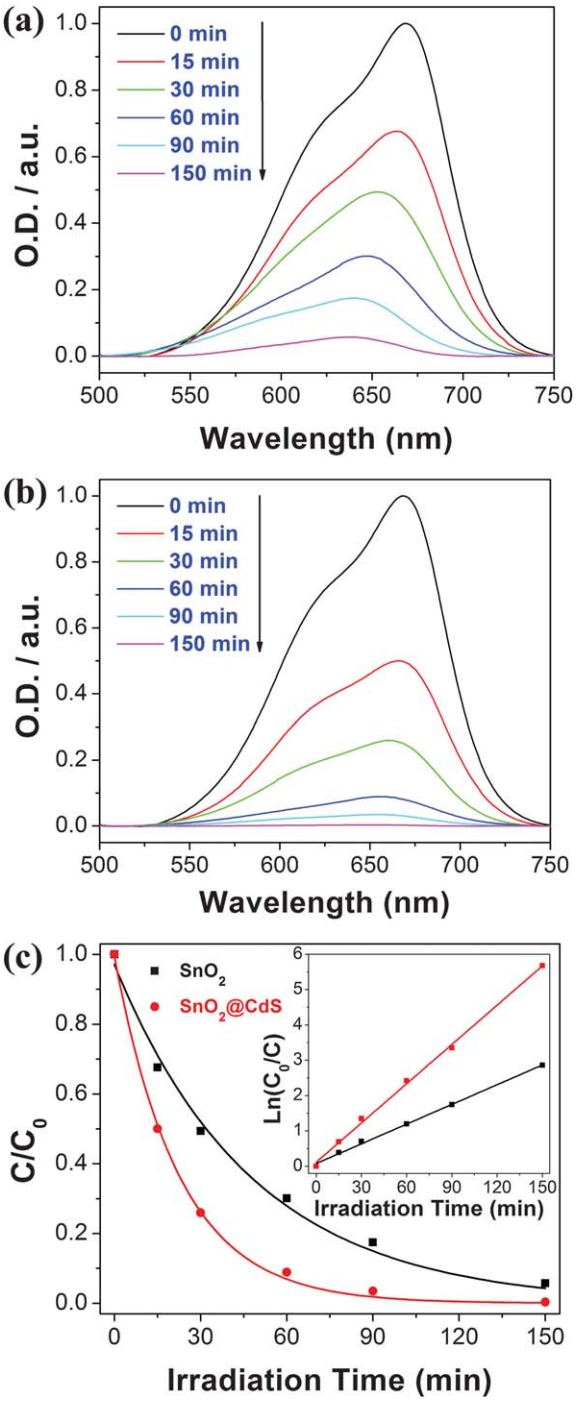

Fig. 6 Absorption spectra of methylene blue solution at different time using (a) SnO_2 nanowires and (b) SnO_2@CdS nanowire heterostructures as the photocatalyst. (c) Decrease of concentration as a function of irradiation time. A natural logarithm C_0/C fitting curves are inserted.

Conclusions

In summary, we have demonstrated a rationally designed SnO_2@CdS nanowire-QDs heterostructures by a chemical bath deposition method *via* hydroxide cluster growth mechanism. Due to the quantum dot decorations, SnO_2@CdS nanowire heterostructures show considerably higher absorption in visible region. Single SnO_2@CdS nanowire heterostructure field-effect transistor device exhibites six times higher photoconductance compared to pristine SnO_2 nanowire devices, suggesting improved solar harvesting power and carrier injection from CdS quantum dots to SnO_2 nanowire backbones. As a conceptual demonstration, we further show that photocatalytic activity of the SnO_2@CdS nanowire heterostructures can be enhanced by nearly 109%. Our findings suggest considerable potentials of SnO_2@CdS nanowire heterostructure for high-sensitivity nanoscale visible-light photodetectors and high efficiency photocatalysis.

Acknowledgements

We gratefully acknowledge financial support by Program for New Century Excellent Talents in University (NECT-2012-0553), Hunan Outstanding Young Teachers Program, and Program for Shenghua Overseas Talents (1681-7601110203) from Central South University (CSU). The authors are thankful to Dr. Jun Zhang, Mr. Dehui Li for their contributions for optical and photocurrent measurements. J. P. is thankful to Prof. Sanjay Mathur (University of Cologne, Germany) and Prof. Qihua Xiong and Mr. Muhammad Iqbal (Nanyang Technological University, Singapore) for fruitful scientific discussions.

References

1 H. Q. Yan, R. R. He, J. Johnson, M. Law, R. J. Saykally and P. D. Yang, *J. Am. Chem. Soc.*, 2003, **125**, 4728–4729.
2 M. Law, L. E. Greene, J. C. Johnson, R. Saykally and P. D. Yang, *Nat. Mater.*, 2005, **4**, 455–459.
3 D. J. Norris, K. S. Leschkies, R. Divakar, J. Basu, E. Enache-Pommer, J. E. Boercker, C. B. Carter, U. R. Kortshagen and E. S. Aydil, *Nano Lett.*, 2007, **7**, 1793–1798.
4 M. Law, D. J. Sirbuly, J. C. Johnson, J. Goldberger, R. J. Saykally and P. D. Yang, *Science*, 2004, **305**, 1269–1273.
5 R. D. Schaller, M. Sykora, J. M. Pietryga and V. I. Klimov, *Nano Lett.*, 2006, **6**, 424–429.
6 A. Kongkanand, K. Tvrdy, K. Takechi, M. Kuno and P. V. Kamat, *J. Am. Chem. Soc.*, 2008, **130**, 4007–4015.
7 J. Pan, M. I. Utama, Q. Zhang, X. Liu, B. Peng, L. M. Wong, T. C. Sum, S. Wang and Q. Xiong, *Adv. Mater.*, 2012, **24**, 4151–4156.
8 Z. Wang, X. Zhan, Y. Wang, S. Muhammad, Y. Huang and J. He, *Nanoscale*, 2012, **4**, 2678–2684.
9 Y. Li, J. Hensel, G. M. Wang and J. Z. Zhang, *Nano Lett.*, 2010, **10**, 478–483.
10 Y. Li, G. M. Wang, X. Y. Yang, F. Qian and J. Z. Zhang, *Nano Lett.*, 2010, **10**, 1088–1092.
11 G. M. Whitesides and G. W. Crabtree, *Science*, 2007, **315**, 796–798.
12 J. B. Sambur and B. A. Parkinson, *J. Am. Chem. Soc.*, 2010, **132**, 2130–2131.
13 Z. A. Peng and X. G. Peng, *J. Am. Chem. Soc.*, 2001, **123**, 183–184.
14 J. Pan, H. Shen, U. Werner, J. D. Prades, F. Hernandez-Ramirez, F. Soldera, F. Mucklich and S. Mathur, *J. Phys. Chem. C*, 2011, **115**, 15191–15197.
15 J. Pan, R. Ganesan, H. Shen and S. Mathur, *J. Phys. Chem. C*, 2010, **114**, 8245–8250.
16 Y. Idota, T. Kubota, A. Matsufuji, Y. Maekawa and T. Miyasaka, *Science*, 1997, **276**, 1395–1397.
17 M. Gratzel, *Nature*, 2001, **414**, 338–344.
18 A. Thissen, J. Fritsche, D. Kraft, T. Mayer, A. Klein and W. Jaegermann, *Thin Solid Films*, 2002, **403**, 252–257.
19 M. A. Hossain, G. W. Yang, M. Parameswaran, J. R. Jennings and Q. Wang, *J. Phys. Chem. C*, 2010, **114**, 21878–21884.
20 M. A. Hossain, J. R. Jennings, Z. Y. Koh and Q. Wang, *ACS Nano*, 2011, **5**, 3172–3181.
21 K. Yong, Y. Tak, S. J. Hong and J. S. Lee, *Cryst. Growth Des.*, 2009, **9**, 2627–2632.
22 J. Pan, J. Zhang, H. Shen, Q. H. Xiong and S. Mathur, *J. Phys. Chem. C*, 2011, **115**, 22225–22231.
23 M. I. Utama, Q. Zhang, S. Jia, D. Li, J. Wang and Q. Xiong, *ACS Nano*, 2012, **6**, 2281–2288.
24 Q. H. Xiong, J. G. Wang, O. Reese, L. C. L. Y. Voon and P. C. Eklund, *Nano Lett.*, 2004, **4**, 1991–1996.
25 K. W. Adu, H. R. Gutierrez, U. J. Kim, G. U. Sumanasekera and P. C. Eklund, *Nano Lett.*, 2005, **5**, 409–414.
26 L. Abello, B. Bochu, A. Gaskov, S. Koudryavtseva, G. Lucazeau and M. Roumyantseva, *J. Solid State Chem.*, 1998, **135**, 78–85.
27 C. A. Arguello, D. L. Rousseau and S. P. S. Porto, *Phys. Rev.*, 1969, **181**, 1351–1363.
28 Z. X. Wang, H. Yin, C. Jiang, M. Safdar and J. He, *Appl. Phys. Lett.*, 2012, **101**, 253109.
29 X. N. Wang, H. J. Zhu, Y. M. Xu, H. Wang, Y. Tao, S. Hark, X. D. Xiao and Q. A. Li, *ACS Nano*, 2010, **4**, 3302–3308.
30 Z. X. Wang, X. Y. Zhan, Y. J. Wang, M. Safdar, M. T. Niu, J. P. Zhang, Y. Huang and J. He, *Appl. Phys. Lett.*, 2012, **101**, 073105.
31 H. Kind, H. Q. Yan, B. Messer, M. Law and P. D. Yang, *Adv. Mater.*, 2002, **14**, 158–161.
32 A. Rose in *Concepts in Photoconductivity and Allied Problems*, Krieger Publishing Company, New York, 1978.
33 Y. Jiang, W. J. Zhang, J. S. Jie, X. M. Meng, X. Fan and S. T. Lee, *Adv. Funct. Mater.*, 2007, **17**, 1795–1800.
34 T. Gao, Q. H. Li and T. H. Wang, *Appl. Phys. Lett.*, 2005, **86**, 173105.
35 M. G. Bawendi, P. J. Carroll, W. L. Wilson and L. E. Brus, *J. Chem. Phys.*, 1992, **96**, 946–954.
36 L. Hu, M. Chen, W. Shan, T. Zhan, M. Liao, X. Fang, X. Hu and L. Wu, *Adv. Mater.*, 2012, **24**, 5872–5877.
37 L. Hu, J. Yan, M. Liao, H. Xiang, X. Gong, L. Zhang and X. Fang, *Adv. Mater.*, 2012, **24**, 2305–2309.
38 H. Chen, L. F. Hu, X. S. Fang and L. M. Wu, *Adv. Funct. Mater.*, 2012, **22**, 1229–1236.

39 L. Hu, J. Yan, M. Liao, L. Wu and X. Fang, *Small*, 2011, **7**, 1012–1017.
40 J. S. Jie, W. J. Zhang, Y. Jiang, X. M. Meng, Y. Q. Li and S. T. Lee, *Nano Lett.*, 2006, **6**, 1887–1892.
41 N. V. Joshi, *Photoconductivity: Art, Science, and Technology*, Marcel Dekker, New York, 1990.
42 Y. J. Wang, Z. X. Wang, S. Muhammad and J. He, *CrystEngComm*, 2012, **14**, 5065–5070.
43 J. C. Yu, G. S. Li and D. Q. Zhang, *Chem. Mater.*, 2008, **20**, 3983–3992.
44 J. W. Tang, Z. G. Zou and J. H. Ye, *Chem. Mater.*, 2004, **16**, 1644–1649.
45 J. Pan, S. M. Huhne, H. Shen, L. S. Xiao, P. Born, W. Mader and S. Mathur, *J. Phys. Chem. C*, 2011, **115**, 17265–17269.
46 A. T. Bell, *Science*, 2003, **299**, 1688–1691.